Experiments and simulations of empty and sand-filled aluminum alloy panels subjected to ballistic impact

J.K. Holmen[1], T. Børvik and O.S. Hopperstad

Structural Impact Laboratory (SIMLab) and Centre for Advanced Structural Analysis (CASA), Department of Structural Engineering, Norwegian University of Science and Technology (NTNU), Trondheim, Norway

ABSTRACT

In this study, we use a discrete particle method in combination with finite element analysis to describe the interaction between structures and granular media during ballistic impact. By applying a discrete particle method to model granular materials, issues like mesh distortion and element deletion can be avoided. This paper presents experiments and numerical simulations on the perforation of empty and sand-filled aluminum alloy panels subjected to impacts by small-arms bullets. The simulations of the sand-filled panels were conducted using a combined discrete particle–finite element approach that accounts for the coupling between structure and sand. The ballistic capacity of the sand-filled aluminum panels was more than 40 % higher than that of the empty aluminum panels. Overall, the results from the numerical simulations describe the trends from the experiments. The predicted ballistic capacity of the empty panels was within 5 % of the experimentally determined value and the critical velocity of the sand-filled panels was predicted within 11 % of the experimentally determined critical velocity. The scatter in residual velocity was similar in simulations and experiments. However, in its current form the discrete particle method needs different calibrations for different velocity regimes to obtain accurate description of the sand behavior.

Keywords: Small-arms bullets; Ballistic tests; Discrete particle method; Finite element method; Granular materials; Protective structures; Soil-structure coupling

[1] Corresponding author: + 47 93 04 58 37 (Jens Kristian Holmen)
Email address: jens.k.holmen@ntnu.no (Jens Kristian Holmen)
URL: www.ntnu.edu/casa

1. INTRODUCTION

Extruded aluminum panels are used in a number of engineering structures due to their low weight-to-stiffness ratio. Børvik et al. [1][2] showed experimentally that AA6005-T6 aluminum panels filled with granular materials can be used with success to mitigate the possibly lethal effects of explosions, and impacts by projectiles or debris. The resistance against explosions was simulated with a finite element model where the response of the granular material was approximated by a constitutive model originally intended for foams. However, the foam model was not deemed accurate enough for perforation simulations, so the ballistic behavior was not analyzed numerically in that study. A significant grain-size effect was revealed in ballistic tests with gravel. Here, grains larger than 2 mm were found to have greater resistance against perforation than typical sand with median grain diameter smaller than 2 mm. The material parameters for the AA6005-T6 aluminum panels were determined some years earlier and numerical simulations of ballistic perforation of empty panels by 20 mm ogival-nosed projectiles were presented in Ref. [3].

In the current study we use the same type of AA6005-T6 aluminum panels as were used in Refs. [1][2][3]. They are in the numerical simulations modeled as a continuum with finite elements. The sand is, on the other hand, modeled with a discrete particle method as rigid spherical particles that transfer forces through a penalty-based contact formulation. This method was proposed by Olovsson et al. [4][5] and was initially developed to handle the gas–fabric contact issues in airbag-deployment simulations before it was applied to represent close-range blast loading and the interaction between high explosives, air, and sand. The discrete particle method is available in the explicit nonlinear finite element code IMPETUS Afea Solver [6] and it was thoroughly described and used for combined sand impact and blast loading on structures by Børvik et al. [7] and Wadley et al. [8]. More recently, Holloman et al. [9][10] applied this discrete particle method to gain insight into the impulse transfer between sand ejecta from

buried charges and structural components. The case of deep penetration by small-arms bullets into granular materials was studied in detail by Børvik et al. [11] and the results from these simulations showed that the method was able to describe several experimentally observed phenomena.

Discrete numerical modeling of granular materials has been researched extensively since Cundall and Strack [12] presented their distinct element model in 1979. Combined discrete particle–finite element approaches like the one presented above have been used, e.g. by Oñate and Rojek [13]. Solid materials such as rock and concrete can also be represented by discrete particles by introducing a cohesive law between individual particles [14]. On an even lower scale, agglomerates of discrete sub-particles can represent larger particles to model cracking and fracture in granular materials as shown by Cil and Alshibli [15]. Discrete particle methods have the advantage of needing relatively few input parameters and the complicated bulk material behavior arises as a consequence of relatively simple assumptions on the particle level [16]. Continuum models, on the other hand, require constitutive equations for the bulk sand and numerical issues might arise in the mesh discretization and with element erosion. Individual sand grains can in some cases be represented by finite elements to allow for crushing. This has been shown to be important in high velocity penetration of sand [17][18][19], but the added complexity comes at a significant computational cost.

High strain rate behavior of sand and its behavior during rapid penetration has been carefully reviewed by Omidvar et al. [20][21]. It is clear from centuries of research that the resistance of sand against a high-velocity intruder such as a bullet is affected by a myriad of parameters on several scales. The most relevant for perforation problems are the shape, trajectory, obliquity, mass and velocity of the bullet; and the density, packing density, grain size and moisture content of the sand. In addition, the frictional effects between the bullet and the sand come into play.

The objective of this study is to evaluate a numerical technique for design of protective structures consisting of sand in combination with ordinary solid materials. To this end we first experimentally determine to which degree filling an aluminum panel with sand increases its capacity against perforation by small-arms bullets; we present a simple calibration method for the discrete particle method; and lastly we use the calibrated discrete particle method in combination with finite elements in an attempt to simulate the entire problem including the sand–structure interaction. By using this approach, we can describe, at least qualitatively, the response of protective structures consisting of a combination of a solid structure and a discrete filling.

2. EXPERIMENTAL STUDY

2.1 Component test setup

All the ballistic tests were conducted in a ballistic laboratory where a smooth-bored 7.62×63 mm Mauser rifle launched the armor piercing (AP) bullets shown in Figure 1 toward the target panels shown in Figure 2 at predefined approximate velocities between 400 m/s and 900 m/s. The nominal mass of the complete bullet was 10.5 g and it consisted of a brass jacket, a lead cap and an ogive-nosed hardened steel core with a nominal mass of 5.0 g, a caliber radius head (CRH) of 3 and a Rockwell C hardness of 63. During testing, 300 mm long sections of the panels were mounted in a rigid frame, and only the bottom and top 30 mm were constrained in the direction of perforation. For the impact conditions considered here the boundary conditions are believed to be of minor importance. The impact point was chosen 27.5 mm from the center line of the panel as indicated in Figure 2, meaning that the projectile also had to perforate the oblique web. For the tests without any sand, at most 10 shots were fired at a 300 mm high profile, leaving 50 mm between each shot. For the remaining tests, sand was filled inside the cavities of similar profiles and the sides of the panels were gently tapped with a rubber hammer

to compact the sand. The panels were mounted on a specially designed steel plate and another steel plate was put on top of the panels before each test. At least 70 mm was left between each impact point and the sand was replaced at irregular intervals. Small pitch angles, $\alpha \leq 3°$, were observed in some of the tests. This is commented upon in Section 3. No spin was given to the bullet, the effects of which were commented on by Børvik et al. [11]. Initially, 49 tests were performed, but nine additional tests were conducted on the B95 sand (see Section 2.2) to further investigate the repeatability of the test setup, giving 58 component tests in total.

Two Phantom v1610 high-speed video cameras were used to capture the perforation process. A Nikon 80-200 1:2.8D lens and a Nikon 70-300 1:4.5-5.6G lens were mounted on the cameras, an exposure time of 0.001 ms was used and an area of approximately 150 mm × 75 mm was covered by each camera. Two Cordin Model 659 flashes were used as light sources. A resolution of 512×304 pixels and a frame rate of 80,000 frames per second for both cameras were sufficient to optically measure the initial and residual velocities of the bullets.

2.2 Sand characteristics

Three types of sand delivered from AB Baskarpsand in Sweden were used in this study: B15, B55 and B95 with respective median grain sizes (diameters) of 0.15 mm, 0.55 mm and 0.95 mm. The main constituents of the sand are quartz (SiO_2) and alumina (Al_2O_3), with minor fractions of other elements. B15 consists of 88.5 % quartz and 6.3 % alumina; B55 consists of 90.1 % quartz and 5.3 % alumina; while B95 consists of 77.1 % quartz and 12.5 % alumina. Table 1 provides some material data for the sand. The grain size curves that show the proportion of grains smaller than a certain size are shown in Figure 3 and the grain size distribution is visualized in Figure 4. The moisture content was measured to be less than 0.5 % for all the sand types. Figure 3 and Figure 4 also show that B95 sand is the least uniform material. This means that the porosity is lower than for B55 and B15 which is why the bulk density is highest for this

sand type. The bulk density in Table 1 was measured with a 1000 cm^3 container normally used for concrete aggregates. However, in relation to the additional ballistic tests we measured the bulk density of the B95 sand when it was filled in the aluminum panels just before impact-testing: no measurement differed more than 2 % from the reported value.

2.3 Results from tests on empty aluminum panels

The residual velocities v_r from the tests on the empty aluminum panels plotted against their respective initial velocities v_i are shown in Figure 5. The solid line was calculated from a generalized version of an analytical model originally proposed by Recht and Ipson [22], also called the Lambert and Jonas equation [23],

$$v_r = a\left(v_i^p - v_{bl}^p\right)^{1/p} \tag{1}$$

where the model parameters a and p, as well as the ballistic limit velocity v_{bl} were simultaneously obtained with a least-squared-error fit to the experimental data points. With $a = 0.94$ and $p = 2.06$ the ballistic limit velocity, which is a common ballistic capacity measure, of the empty panels was found to be $v_{bl} = 450.1\,\mathrm{m/s}$.

A total of eleven shots were fired at the empty panels. A cross section showing the penetration channels from two tests is presented in Figure 6. The entry holes were similar for every test and ductile hole enlargement was the main perforation mechanism. No evidence was found of stripping of the brass jacket during perforation of the front plate in any of the tests. The flight trajectory after impact was unstable for low initial velocities. The bullet did in some cases deviate significantly from its initial flight path which was evident from the large spread of the exit holes on the back plate. The bullet instability was amplified by the oblique web and in some cases the bullet made a $90°$ turn inside the aluminum panel and came to a complete stop in the outer oblique web. Generally, the jacket was stripped off by the rear plate.

2.4 Results from tests on sand-filled aluminum panels

The residual velocities v_r from the tests on the sand-filled panels plotted against their respective initial velocities v_i are shown in Figure 7. The figure reveals that there is no one-to-one relationship between v_r and v_i, i.e., the tests are not easily repeatable and the scatter is large. However, it is clear that filling the panels with sand of any kind increased the panel's resistance to perforation as expected. To compare the results to the empty panels we define a combined critical velocity v_{crit} for all the sand-filled panels. If the bullet's initial velocity exceeds v_{crit}, perforation can be expected. This is a conservative estimate, but $v_{crit} = 646.0$ m/s is a 43.5 % increase from the capacity of the empty panels and it clearly illustrates that the capacity can be substantially increased by filling the panels with sand. No clear and significant change in the ballistic limit velocity was found between the three different sand types used in this study.

A panel sliced in half is shown in Figure 8. Contrary to what happened inside the empty panels, the bullet's jacket was normally stripped off between the front plate and the oblique web when the panels were filled with sand. Figure 7 clearly displays that results from perforation of the sand-filled panels are more dispersed than results from perforation of empty aluminum panels in Figure 5. Definite conclusions about the perforation resistance of the three sand types are difficult to draw and have not been emphasized in the ensuing numerical work.

The large scatter in the test data was checked for B95 sand in two test series with an impact velocity of 820 ± 20 m/s: (1) Five shots fired into five separate brand new panels with previously unused sand, and (2) four shots fired into the same panel without changing the sand between the tests. The mean value and scatter of the residual velocity were similar in both test series, indicating that the employed experimental procedure was adequately accurate.

3. NUMERICAL STUDY

3.1 Aluminum panels and 7.62 AP-bullets

A comprehensive study on the material behavior of AA6005-T6 aluminum alloy panels was presented by Børvik et al. [3]. Quasi-static tension tests, pre-notched tension tests, and tension tests at elevated strain rates and temperatures were conducted to calibrate modified versions [24] of the Johnson-Cook (JC) flow stress model and the JC failure model. In the current paper we have used the original model proposed by Johnson and Cook [25] that reads

$$\sigma_{eq} = \left(A + Bp^n\right)\left(1 + c\ln\left(\dot{\varepsilon}\right)\left(\frac{T - T_r}{T_m - T_r}\right)^m\right). \tag{2}$$

A, B and n are hardening parameters, p is the equivalent plastic strain, $\dot{\varepsilon}$ is the plastic strain rate, $\dot{\varepsilon}$ is a reference strain rate, T is the current temperature, T_r is the ambient/room temperature, T_m is the melting temperature, while c and m are parameters controlling the material's strain rate sensitivity and temperature dependency, respectively. The original JC failure criterion [26] was used to model failure of the aluminum panels in this study; the damage parameter D is dependent on the incremental plastic strain Δp as

$$D = \sum \frac{\Delta p}{p_f} \tag{3}$$

and the current plastic failure strain reads

$$p_f = \left(D_1 + D_2 \exp(D_3\sigma^*)\right)\left(1 + D_4 \ln\left(\dot{\varepsilon}\right)\left(D_5\left(\frac{T - T_r}{T_m - T_r}\right)\right)\right). \tag{4}$$

D_1, D_2, D_3, D_4 and D_5 are model parameters, $\sigma^* = \sigma_H / \sigma_{eq}$ is the stress triaxiality ratio and $\sigma_H = (\sigma_1 + \sigma_2 + \sigma_3)/3$ where $\sigma_1 \geq \sigma_2 \geq \sigma_3$ are the ordered principal stresses. All the material and failure parameters for the panels can be found in Table 2. Note that c and D_4 were recalibrated from the values presented in Ref. [3] since the rate-sensitivity terms in the original and modified versions of the JC constitutive models and failure criteria are slightly different. The reason for using the original JC model, and not the modified JC model, is that the modified JC failure model is not implemented in the standard version of IMPETUS Afea Solver.

The 7.62 mm AP bullet has been used in several previous studies by the authors, e.g., [11][27][28]. The hardened steel core was considered as a rigid body with density $\rho = 7850\ \mathrm{kg/m^3}$, while the brass jacket and lead tip were modeled using the original JC constitutive equation presented in Eq. (2). Failure of these parts was controlled by the one-parameter failure criterion proposed by Cockcroft and Latham (CL) [29],

$$D = \frac{1}{W_{cr}} \int_0^p \langle \sigma_1 \rangle \, \mathrm{d}p = \frac{1}{W_{cr}} \int_0^p \left\langle \sigma^* + \frac{3 + \mu_\sigma}{3\sqrt{3 + \mu_\sigma^2}} \right\rangle \sigma_{eq} \, \mathrm{d}p, \qquad \langle \sigma_1 \rangle = \max(0, \sigma_1), \tag{5}$$

where W_{cr} is the failure parameter and σ_1 is the major principal stress. As shown in Eq. (5), the major principal stress can be expressed as a function of the stress triaxiality ratio σ^* and the Lode parameter μ_σ defined here as

$$\mu_\sigma = \frac{2\sigma_2 - \sigma_1 - \sigma_3}{\sigma_3 - \sigma_1} \ . \tag{6}$$

The failure parameter W_{cr} represents an amplified plastic work to failure and can be found from a uniaxial tension test by integrating σ_1 over the entire plastic strain path to specimen failure. Material and failure parameters for the bullet materials can be found in Table 3.

3.2 The discrete particle method

Sand is modeled with a discrete particle method described in more detail by Børvik et al. [7]. The method employs a penalty-based contact formulation where elasticity, friction and damping may all be accounted for. The rheological model, which is similar to a model proposed by Deshpande et al. [30], is shown in Figure 9 and it includes a tangential and a normal spring both with stiffness k_s, a normal dashpot with damping coefficient c_s, and lastly a frictional element with a Coulomb friction coefficient μ_s that controls the tangential elastic spring force. In addition to this a particle–structure friction coefficient μ_{ps} controls the friction between particles and finite elements. Recently, a similar, but augmented, model was employed by Oñate et al. [14] to represent cohesive materials.

The discrete particles are included in the various numerical models by distributing unit cells with 1000 particles of similar size and with periodic particle stacking. Just like the JC flow stress model presented in Section 3.1 the discrete particle method is phenomenological. No attempt is made to describe all the underlying physical processes related to the deformation of the sand; they are instead incorporated in the simulations by adapting parameters to experimental calibration tests as will be done in the following. Phenomena like particle fracture and particle rotation are not modeled explicitly, but accounted for in the calibration of the model through the inter-particle stiffness k_s and friction μ_s. The inter-particle damping c_s was neglected in this study because friction seems to be the dominating energy dissipating mechanism in dry sand; this was discussed in further detail by Børvik et al. [7].

3.3 Calibration of the discrete particle model

Traditional methods of characterizing granular materials undergoing high strain rate loading are complex and require advanced test facilities. Four common testing methods were identified by Omidvar et al. [20]: uniaxial compression tests, Split Hopkinson Pressure Bar tests, triaxial

compression tests and plane wave shock tests. In the current paper, we used a simplified method to characterize the sand which is explained below. The calibration test is similar enough to the component test to capture the most important phenomena without invalidating the prediction of the component behavior by being too similar. An alternative to the proposed calibration procedure would have been to inverse model one of the component tests to demonstrate the features of this discrete particle method.

Calibration of the discrete particles and their constants was done by performing some simple perforation tests of sand slabs contained in a specially designed steel container. The box was 50 mm thick in the impact direction and had inner dimensions of 250 mm × 200 mm in the directions transverse to the flight path. The transverse dimensions of the box were chosen to minimize the effects of the boundaries. Holes with diameter 25 mm were drilled in the front and back walls of the box to create a free passage for the projectile. These holes were covered with 0.1 mm thick domestic aluminum foil before filling the box with sand. Rigid steel balls of diameter 10 mm and with a Rockwell C hardness of 60 were fired from a compressed gas-gun of which more information can be found in Ref. [3]. The initial and residual velocities, v_i and v_r respectively, of the steel balls were measured by a high-speed camera of the same type as described in Section 2.1, now at a resolution of 1280×208 pixels and with a frame rate of 60,000 fps.

The B95 sand with a median grain size of 0.95 mm was used in the calibration tests. A total of 11 tests were conducted at initial velocities between 160 m/s and 360 m/s. These initial velocities ensured significant retardation of the steel ball in the sand. Figure 10 presents the results from the calibration tests while Figure 11 shows a timelapse from the test with $v_i = 279.1\,\text{m/s}$ and $v_r = 65.0\,\text{m/s}$. Three parallel tests were conducted with impact velocities around 278 m/s, while for the other velocities only one test was performed (see Figure 10).

Their average initial and residual velocities ($\overline{v}_i = 278.1$ m/s and $\overline{v}_r = 60.7$ m/s) were chosen as a basis for the following parametric study and calibration procedure.

Figure 12 shows the sand box model that was made in the IMPETUS Afea Solver to study the influence of the particle size, inter-particle friction and stiffness, and the particle–structure friction. The default parameters for the generic dry sand that are available in IMPETUS Afea Solver [6][7] are listed in Table 4; these were used in the investigation of particle size. The effect of particle–structure friction was neglected in this particular parametric study. In Ref. [11] it was found that particles somewhat larger than the median grain size of the sand would produce good results while limiting the computational time. Simulations with 50,000 to 8,000,000 particles were run with an otherwise identical model. The average particle diameter then varied from 1.93 mm to 0.415 mm and the solid volume fraction was constant at 0.6. Figure 13 shows the residual velocity plotted as a function of the number of particles. It is clear that the resistance against perforation decreases by increasing the number of particles. A total of 830,000 discrete particles were chosen for subsequent calibration, i.e., a particle diameter of approximately 1.5 mm will be used in the rest of this paper.

Individual effects of inter-particle friction μ_s and particle–structure friction μ_{ps} were also investigated and the results are shown in Figure 14. We find that by increasing either of the friction parameters we increase the resistance against perforation. The residual velocity is more sensitive to the inter-particle friction than to the particle–structure friction. The inter-particle stiffness was also varied, but the effect was small compared to the friction and we decided to keep the default stiffness value $k_s = 4.0 \times 10^8$ N/m.

Based on the preceding discussion it appears that several parameter combinations can give the same residual velocities. We have chosen a combination of inter-particle friction $\mu_s = 0.225$ and particle–structure friction $\mu_{ps} = 0.2$ for the main study in this paper. By considering three

different impact positions (± 1 mm) we get results within 7 % of the experimental average. The numerical average, however, is identical to the experimental average. Table 4 summarizes the calibrated constants for the discrete particle model. A numerical simulation of the calibration model is shown in Figure 15, and comparing this figure to Figure 11 reveals that the model is capable of qualitatively describing the experimental behavior.

The discrete particle method applied in this work has so far mainly been tested for rather high impact velocities between 150 m/s and 1000 m/s. The calibration tests reported above have been done within the velocity domain where the method has previously been used, but at a lower velocity than in the component tests. We used only one impact velocity to calibrate the DPM, but as can be seen in Figure 10, we conducted 11 tests. Unfortunately, the model was not capable of exactly predicting the residual velocity for all the impact tests. To investigate the sensitivity of the chosen calibration velocity we ran simulations to find parameter sets that would match the calibration tests at the lowest ($v_i = 165.2$ m/s and $v_r = 23.4$ m/s) and highest ($v_i = 356.9$ m/s and $v_r = 96.7$ m/s) impact velocities. Only the inter-particle friction μ_s was varied in this sensitivity study because it was found to be more important than the particle–structure friction μ_{ps}. After some trial and error, we found $\mu_s = 0.35$ for the lowest impact velocity and $\mu_s = 0.175$ for the highest impact velocity. These parameters will also be used in the subsequent simulations of the full component tests.

3.4 Numerical models

A numerical model of the AA6005-T6 aluminum panel was made based on the geometry in Figure 2. The mesh is shown in Figure 16. Some simplifications were made in the finite element discretization: we included only 200 mm of the panel in the extrusion direction and the geometry near the panel's corners was simplified. These alterations are not expected to affect the results. In the impact region fully integrated 3rd-order 64-node hexahedral elements of

approximate size 1 mm × 1 mm × 1 mm were chosen while in the peripheral parts of the panel the mesh was coarser and the elements were linear 8-node hexahedrons. No significant change in the residual velocity was seen with a finer discretization. The bullet was discretized with only the 3rd-order 64-node hexahedral elements. Such higher-order elements are available in the IMPETUS Afea Solver and they have been applied previously in other perforation studies [27][28]. A more thorough description of the higher order elements can be found in Holmen et al. [31]. The calibration of the discrete particle method in Section 3.3 was based on a grain diameter of 1.5 mm. To obtain the same diameter in the simulations of the component tests 1,460,000 particles were used.

The material parameters determined in Sections 3.1-3.3 and listed in Table 2, Table 3 and Table 4 were used in most of the simulations. Elements in the bullet are removed from the analysis when 16 out of their 64 integration points reach $D = 1$ as defined in Eq. (5) or when the stable time step drops below 5 ns. For the elements in the aluminum panel the deviatoric resistance in an integration point is removed when $D = 1$ as defined in Eq. (3), but the element is not removed from the analysis until its stable time step reaches a value of 3 ns. Friction between the bullet and the panel exists and might be of significance, but it is disregarded in these simulations. By omitting frictional effects, the velocity at which the bullet strikes the sand will be higher. This will most likely give higher residual velocities.

Impact velocities for the empty aluminum panels were chosen in regular intervals between 400 m/s and 900 m/s to be able to predict the ballistic limit curve and the ballistic limit velocity v_{bl}. For the sand-filled panels, the impact velocity was chosen between 550 m/s and 900 m/s because of the increased resistance from the sand. Sensitivity studies regarding the bullet's impact point and pitch angle were also conducted. In this study we adopt the definitions from Goldsmith [32] where the pitch α is the angle between the bullet's centerline and the velocity vector as shown in Figure 17.

3.5 Numerical results

Figure 18 shows the simulation results for the empty aluminum panels compared to the ballistic tests reported in Section 2.3. For the simulations with no initial pitch angle, i.e., normal impact, the residual velocities were slightly overestimated, meaning that the ballistic limit velocity was underestimated. The difference from the experiments is, however, only 4.2 %. For initial velocities close to the ballistic limit velocity a positive pitch angle gives slightly lower residual velocities. Conversely, a negative pitch angle gives slightly higher residual velocities. A typical timelapse of the perforation process is shown in Figure 19. We observe that the lead cap was completely eroded before perforation of the oblique web and that the brass jacket was nearly stripped off the rigid core after complete perforation of the panel. For this particular velocity we also see that the bullet turned towards the oblique web during perforation which was also found in some of the experimental tests, see Figure 6. For lower impact velocities, the bullet turned in the opposite direction during perforation displayed for $v_i = 500$ m/s in Figure 20, where we also see that below the ballistic limit velocity the bullet turned completely and in some cases it did not even reach the rear plate, just as in the experimental tests.

In Figure 21 the results from the numerical simulations of the sand-filled aluminum panels are compared to the results from the ballistic tests reported in Section 2.4. Various impact points and pitch angles have been considered. The critical velocity was found to be 575.0 m/s. This is an 11 % underestimation of the experimental value. For higher impact velocities the results are within the experimental scatter. In the experiments the brass jacket was stripped off between the front plate and the oblique web in most of the tests. In the simulations with high initial velocities the jacket was stripped off by the oblique web, while at lower velocities it was stripped off between the oblique web and the rear plate. Figure 22 shows a typical timelapse of the perforation process after normal impact. The direction in which the bullet turns during perforation seems somewhat arbitrary in these simulations and they, to some extent, capture the

effect of random particle stacking from the experiments. Figure 23 shows a picture from a simulation where the bullet's impact point was moved 0.5 mm; this is denoted *seed 2* in Figure 21. The initial velocity was identical as in Figure 22 (700 m/s); however, the bullet turned in the opposite direction after perforation for *seed 2*. Note that the residual velocities for the two striking points are fairly different. It was found that the residual velocity is markedly influenced by the trajectory of the bullet through the component, as also observed in [11].

A direct qualitative comparison between an experiment and a numerical simulation is given in Figure 24. The experiment was performed with B95 sand and the sand has been suppressed from the simulation to improve visualization. These pictures show that the failure mechanisms from the experiment can be reproduced by the simulation. Figure 24 further suggests that the proposed method can be used to describe the most important experimental observations within the given impact velocity range.

Lastly, the robustness of the calibration procedure in Section 3.3 is examined. As shown in Figure 10, the parameter set used in the simulations of the component tests gave residual velocities in the calibration tests that were too high for the lowest impact velocities and too low for the highest ones. An initial velocity of 800 m/s was chosen to investigate implications of the alternative parameter sets on the results of the component tests. It was found that a reduction of the inter-particle friction coefficient μ_s to 0.175 increased the residual velocity by about 27 %. Conversely, an increase of μ_s to 0.35 decreased the residual velocity by about 12 %. As the current version of the model is not capable of describing accurately the results in the calibration tests over the applied velocity range, it was necessary to select one impact velocity to obtain the parameter set. The above simulations illustrate a weakness of the discrete particle method which has to be remedied in further work.

4. DISCUSSION

Experimental observations from the current study confirm the conclusions made by Børvik et al. [1][2] that filling panels with granular materials significantly increases the perforation capacity. Ref. [1][2] also revealed that if the grain size is about the same as, or larger than, the projectile, the perforation resistance of the component is significantly improved compared to cases where the grains are much smaller than the projectile. In the current study we did not find conclusive evidence to decide which sand-type gave the highest capacity, probably because the bullet is an order of magnitude larger than the median grain size of the sands investigated here.

Perforation simulations of sand-filled aluminum profiles, or granular materials of any kind, are complex, and a certain initial velocity does not necessarily give the same residual velocity in consecutive experiments due to the influence of individual grains, variations in density, etc. Figure 21 shows that this behavior was to some extent captured in the simulations since moving the impact point 0.5 mm or tilting the bullet by an angle of 3° in some cases changed the residual velocity considerably. It is also clear from the calibration simulations in Section 3.3 that the particle size affects the residual velocity of the rigid steel balls and consequently the resisting force from the discrete particles on the penetrator; larger particles give larger forces.

The explicit non-linear finite element method using Lagrangian meshes is prevalent when analyzing the response of solid structures subjected to ballistic impact. Although a Lagrangian mesh provides convenient treatment of complicated boundary conditions and history-dependent variables, difficulties arise when the deformations become too extreme resulting in small time steps and possibly inverted elements. In granular materials, the individual grains shuffle around and switch places during penetration, which makes simulation using Lagrangian finite element meshes more challenging. Recognizing that the behavior of sand is not directly dependent upon history variables, a coupled approach like the one presented herein seems to be well-suited to represent the sand in explicit simulations with discrete particles where structural components

are modeled with conventional finite elements. It is apparent from the results presented in Section 3 that the DPM is capable of describing the penetration and perforation behavior rather successfully, but for considerably lower impact velocities, other mechanisms seem to dominate the energy dissipation process. This requires a different friction description or, at least, another calibration of the model. Modifying the rheological model is outside the scope of this work where the main objective has been to evaluate the capabilities of the current version of the discrete particle method.

5. CONCLUDING REMARKS

This study first presented experiments on the perforation resistance of empty and sand-filled aluminum alloy AA6005-T6 panels impacted by 7.62 mm AP-bullets. A ballistic limit velocity of 450.1 m/s was found for the empty panels. Subsequent tests were done where sand with a median grain diameter of either 0.15 mm, 0.55 mm or 0.95 mm was filled in the panel's cavities prior to testing. The added resistance from the sand resulted in a 43.5 % increase in the capacity regardless of the type of sand used as filling material.

Numerical simulations were carried out using a coupled discrete particle–finite element approach. Finite elements were used to represent the aluminum panels while discrete particles were used to represent the sand. The following observations were made: Simulations of the empty aluminum panels predicted the perforation process and the capacity of the panels within 5 % of the experimental values confirming that the behavior of the aluminum panels was adequately captured. The critical perforation capacity of the sand-filled panels was predicted within 11 % of the critical velocity from the experiments, a good result when we recognize the complexity of the problem. Numerical simulations of protective structures consisting of a combination of granular and solid materials are challenging and require robust and advanced numerical algorithms. Although the presented method gives good results within the limitations

of this study, some challenges remain. First, the method should be validated for low-velocity impacts. Second, and more importantly, the discrete particle method should be further developed to enable simulation of both low and high velocity impacts using the same parameter set. Nevertheless, the results presented in this paper suggest that coupled discrete particle–finite element methods can be used in engineering design processes and serve as a useful tool for research purposes.

ACKNOWLEDGMENT

The financial support for this work comes from the Structural Impact Laboratory (SIMLab) at the Norwegian University of Science and Technology, The Research Council of Norway, and from the Norwegian Defense Estates Agency (NDEA). The authors would also like to express their gratitude to MSc-students Fredrik R. Bjerke and Lars M. Hansen for their help with the experimental work. Dr. Lars Olovsson from IMPETUS Afea Solver AB is also gratefully acknowledged.

REFERENCES

[1] Børvik T, Hanssen AG, Dey S, Langberg H, Langseth M. On the ballistic and blast load response of a 20 ft ISO container protected with aluminium panels filled with a local mass - Phase I: Design of protective system. Engineering Structures 2008; 30; 1605-1620.

[2] Børvik T, Burbach A, Langberg H, Langseth M. On the ballistic and blast load response of a 20 ft ISO container protected with aluminium panels filled with a local mass – Phase II: Validation of protective system. Engineering Structures 2008; 30; 1621-1631.

[3] Børvik T, Clausen AH, Eriksson M, Berstad T, Hopperstad OS, Langseth M. Experimental and numerical study on the perforation of AA6005-T6 panels. International Journal of Impact Engineering 2005; 32; 35-64.

[4] Olovsson L. Corpuscular Method for Airbag Deployment Simulations in LS-DYNA. IMPETUS Afea AB, Huddinge (ISBN 978-82-997587-0-3).

[5] Olovsson L, Hanssen AG, Børvik T, Langseth M. A particle-based approach to close-range blast loading. European Journal of Mechanics A/Solids 2010; 29; 1-6.

[6] IMPETUS Afea AS. IMPETUS Afea Solver: http://www.impetus-afea.com [cited: 2015-03-01].

[7] Børvik T, Olovsson L, Hanssen AG, Dharmasena KP, Hansson E, Wadley HNG. A discrete particle approach to simulate the combined effect of blast and sand impact loading of steel plates. Journal of the Mechanics and Physics of Solids 2011; 59; 950-958

[8] Wadley HNG, Børvik T, Olovsson L, Wetzel JJ, Dharmasena KP, Hopperstad OS, Deshpande VS, Hutchinson JW. Deformation and fracture of impulsively loaded sandwich panels. Journal of the Mechanics and Physics of Solids 2013; 61; 674-699.

[9] Holloman RL, Deshpande V, Wadley HNG. Impulse transfer during sand impact with a solid block. International Journal of Impact Engineering 2015; 76; 98-117.

[10] Holloman RL, Deshpande V, Wadley HNG. Impulse transfer during sand impact with a cellular structure. International Journal of Impact Engineering 2015; 82; 36-58.

[11] Børvik T, Dey S, Olovsson L. Penetration of granular materials by small-arms bullets. International Journal of Impact Engineering 2015; 75; 123-139.

[12] Cundall PA, Strack ODL. A discrete numerical model for granular assemblies. Géotechnique 1979; 1; 47-65

[13] Oñate E, Rojek J. Combination of discrete element and finite element methods for dynamic analysis of geomechanics problems. Computer Methods in Applied Mechanics and Engineering 2004; 193; 3087-3128.

[14] Oñate E, Zárate F, Miquel J, Santasusana M, Celigueta MA, Arrufat F, Gandikota R, Valiullin K, Ring L. A local constitutive model for the discrete element method. Application to geomaterials and concrete. Computational Particle Mechanics 2015; 2; 139-160.

[15] Cil MB, Alshibli KA. 3D assessment of fracture of sand particles using discrete element method. Géotechnique Letters 2012; 2; 161-166.

[16] Cundall PA. A discontinuous future for numerical modelling in geomechanics? In: Proceedings of the Institution of Civil Engineers. Geotechnical Engineering 149. Issue 1. 2001, p. 41-47.

[17] Braslau D. Partitioning of energy in hypervelocity impact against loose sand target. Journal of Geophysical Research 1970; 75; 3987-3999.

[18] Parab ND, Claus B, Hudspeth MC, Black JT, Mondal A, Sun J, Fezzaa K, Xiao X, Luo SN, Chen W. Experimental assessment of fracture of individual sand particles at different loading rates. International Journal of Impact Engineering 2014; 68; 8-14.

[19] Omidvar M, Malioche JD, Bless S, Iskander M. Phenomenology of rapid penetration into granular soils. International Journal of Impact Engineering 2015; 85; 146-160.

[20] Omidvar M, Iskander M, Bless S. Stress-strain behavior of sand at high strain rates. International Journal of Impact Engineering 2012; 49; 192-213.

[21] Omidvar M, Iskander M, Bless S. Response of granular media to rapid penetration. International Journal of Impact Engineering 2014; 66; 60-82.

[22] Recht RF, Ipson TW. Ballistic perforation dynamics. Journal of Applied Mechanics 1963; 30; 384-390.

[23] Zukas JA (Editor), 1982. *Impact Dynamics*, John Wiley & Son, New York.

[24] Børvik T, Hopperstad OS, Berstad T, Langseth M. A computational model of viscoplasticity and ductile damage for impact and penetration. European Journal of Mechanics – A/Solids 2001; 5; 685-712.

[25] Johnson GR, Cook WH. A constitutive model and data for metals subjected to large strains, high strain rates and high temperatures. In: Proceedings of the 7th International Symposium on Ballistics. 1983, p. 541-547.

[26] Johnson GR, Cook WH. Fracture characteristics of three metals subjected to various strains, strain rates, temperatures and pressures. International Journal of Engineering Fracture Mechanics 1985; 21; 31-48.

[27] Børvik T, Olovsson L, Dey S, Langseth M. Normal and oblique impact of small arms bullets on AA6082-T4 aluminium protective plates. International Journal of Impact Engineering 2011; 38; 577-589.

[28] Holmen JK, Johnsen J, Jupp S, Hopperstad OS, Børvik T. Effects of heat treatment on the ballistic properties of AA6070 aluminium alloy. International Journal of Impact Engineering 2013; 57; 119-133.

[29] Cockcroft MG, Latham DJ. Ductility and the workability of metals. Journal of the Institute of Metals 1968; 96; 33-39.

[30] Deshpande VS, McMeeking RM, Wadley HNG, Evans AG. Constitutive model for predicting dynamic interactions between soil ejecta and structural panels. Journal of the Mechanics and Physics of Solids 2009; 57; 1139-1164.

[31] Holmen JK, Johnsen J, Hopperstad OS, Børvik T. Influence of fragmentation upon the capacity of aluminum alloy plates subjected to ballistic impact. European Journal of Mechanics – A/Solids 2016; 55; 221-233.

[32] Goldsmith W. Non-ideal projectile impact on targets. International Journal of Impact Engineering 1999; 22; 95-395.

TABLES

Table 1: Material properties for the sand

Sand type	Median grain size (mm)	Compacted density (kg/m^3)	Particle density (kg/m^3)	Moisture content (%)
B15	0.15	1629	2600-2700	0.42
B55	0.55	1695	2600-2700	0.32
B95	0.95	1731	2600-2700	0.30

Table 2: Model constants for the aluminum alloy AA6005-T6 panel [3].

A (MPa)	B (MPa)	n	D_1	D_2	D_3	D_4 [2]	D_5	m
270.0	134.0	0.514	0.06	0.497	-1.551	0.0329	6.80	0.703
E (MPa)	ν	ρ (kg/m^3)	c [3]	$\dot{\varepsilon}_1$ (s^{-1})	C_p (J/kg K)	α (K^{-1})	T_r (K)	T_m (K)
70,000	0.3	2700.0	0.0086	1×10^{-3}	910.0	2.3×10^{-5}	293	893

Table 3: Model constants for the bullet materials [27].

	A (MPa)	B (MPa)	n	W_{cr} (MPa)	$\dot{\varepsilon}_1$ (s^{-1})	c [4]	m
Lead tip	24.0	300.0	1.0	175.0	5×10^{-4}	0.2293	1.0
Brass jacket	206.0	505.0	0.42	914.0	5×10^{-4}	0.0108	1.68
	E (MPa)	ν	ρ (kg/m^3)	C_p (J/kg K)	α (K^{-1})	T_r (K)	T_m (K)
Lead tip	10,000	0.42	10,660	124	2.9×10^{-5}	293.0	760.0
Brass jacket	115,000	0.31	8520	385	1.9×10^{-5}	293.0	1189.0

[2] Modified from the original value of 0.0286 due to the change from a power term to a logarithmic term
[3] Modified from the original value of 0.0082 due to the change from a power term to a logarithmic term.
[4] Modified from 0.1 to 0.2293 and 0.01 to 0.0108 respectively due to the change from a power term to a logarithmic term.

Table 4: The model constants for the discrete particle model

	ρ_s (kg/m^3)	k_s (N/m)	μ_s	μ_{ps}	c_s
Generic dry sand	1620.0	4.0×10^8	0.1	0.0	0.0
Calibrated values used in this paper	1731.0	4.0×10^8	0.225	0.2	0.0

FIGURES

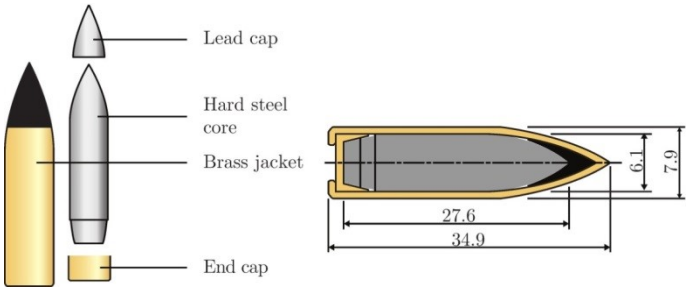

Figure 1: Geometry of the AP-bullet used in this study.

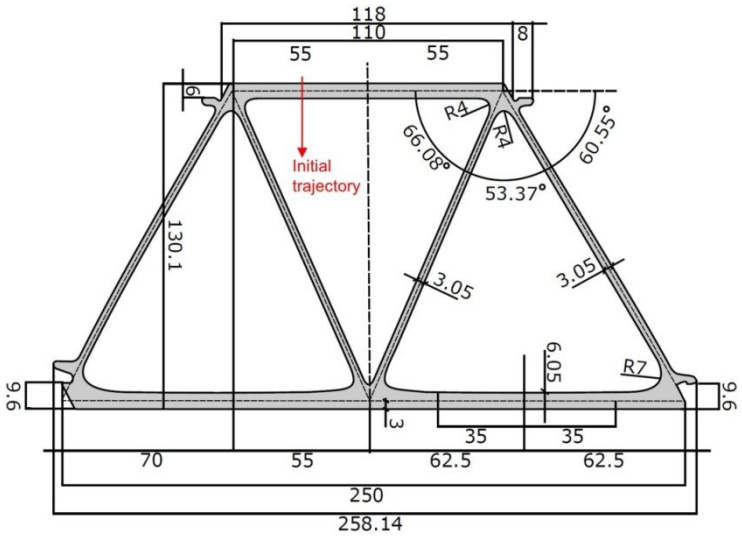

Figure 2: Geometry of the AA6005-T6 aluminum panel and an indication of the initial bullet trajectory/impact point.

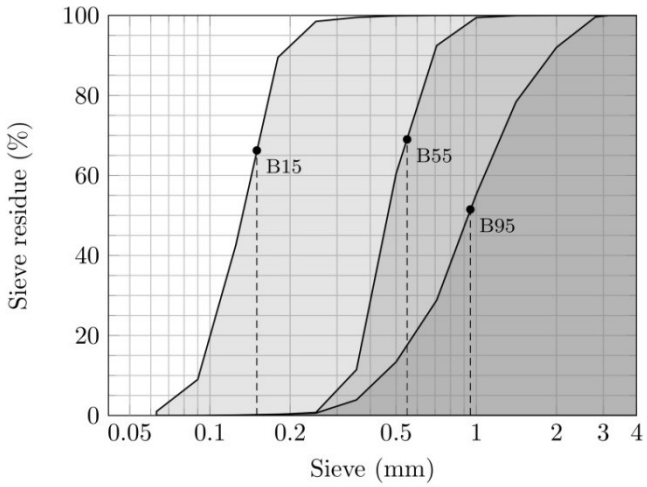

Figure 3: Grain size curves for the three sand types. The median grain sizes are indicated with dashed lines.

(a) B15 (b) B55 (c) B95

Figure 4: Visualization of the grain size distribution for the three sand types.

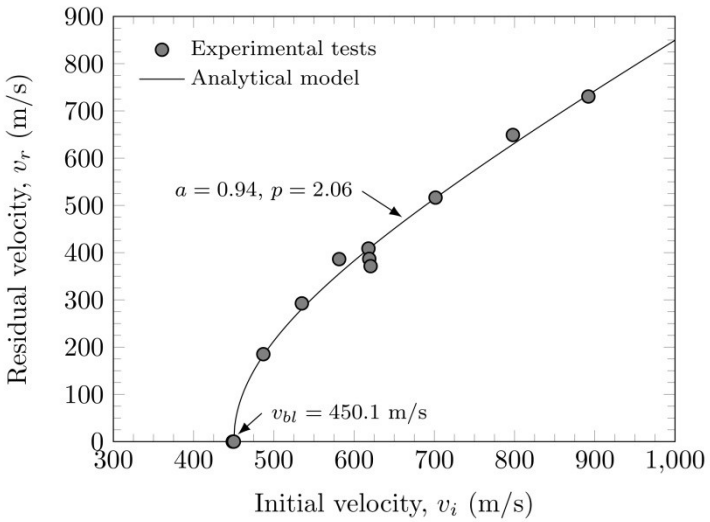

Figure 5: Results from ballistic tests of the AA6005-T6 aluminum alloy panels without sand.

Figure 6: Cross section of an AA6005-T6 panel that was struck without sand. Left: $v_i = 618.9$ m/s and $v_r = 386.3$ m/s. Right: $v_i = 534.9$ m/s and $v_r = 292.6$ m/s.

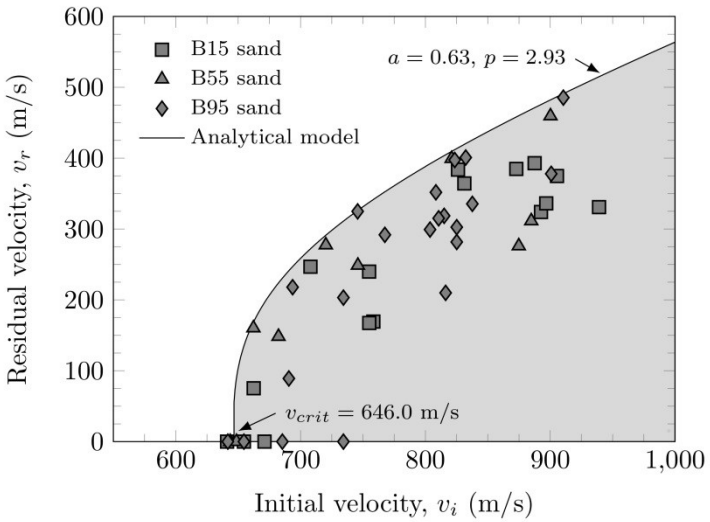

Figure 7: Results from ballistic tests of the AA6005-T6 aluminum alloy panels filled with the three different sand types. Each test is identified by a mark, while the gray area represents the unsafe domain where perforation can be expected.

Figure 8: Cross section of an AA6005-T6 panel that was struck when filled with B95 sand: $v_i = 910.5\,\text{m/s}$ and $v_r = 485.4\,\text{m/s}$.

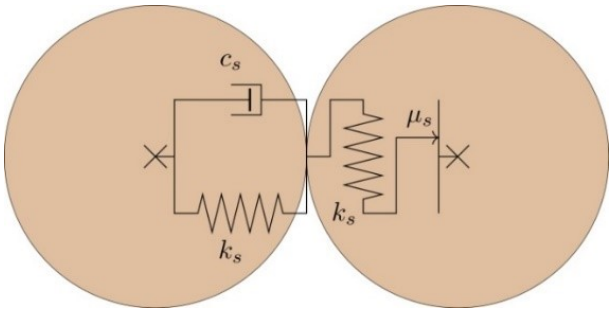

Figure 9: Rheological model for the discrete particles

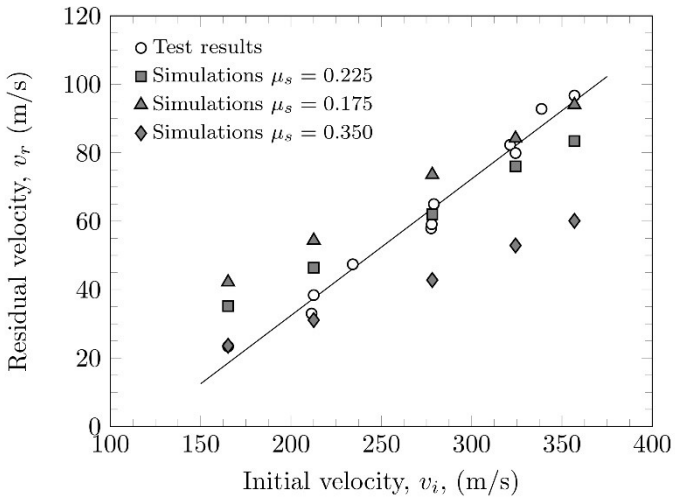

Figure 10: Results from the calibration procedure. The particle–structure friction is $\mu_{ps} = 0.2$ for the simulations plotted here.

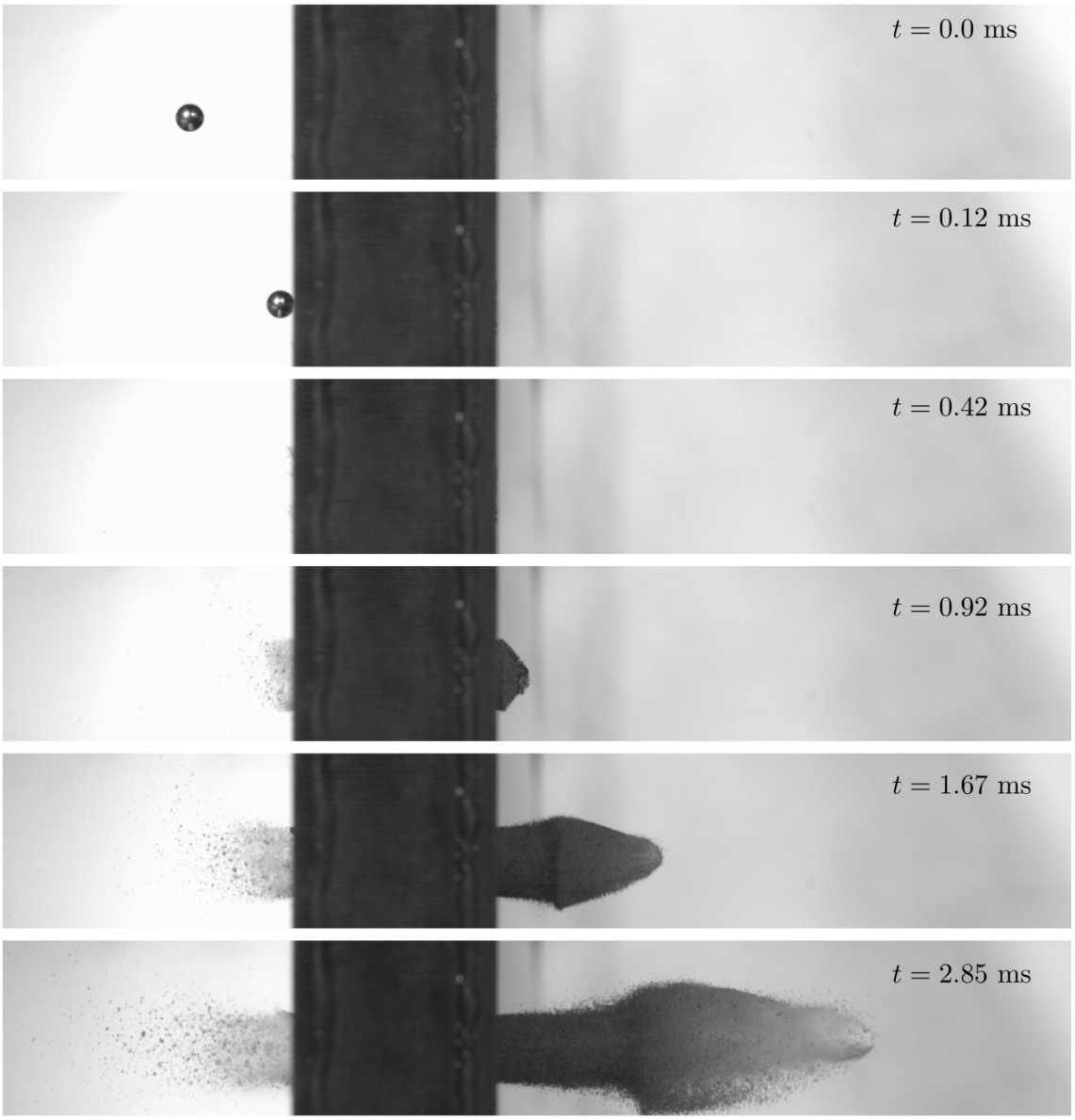

Figure 11: Timelapse from calibration test 3, $v_i = 279.1\,\text{m/s}$ and $v_r = 65.0\,\text{m/s}$.

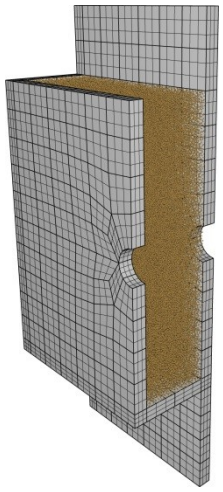

Figure 12: Simulation model of the steel box used in the calibration analyses. Only half the model is shown to improve visualization.

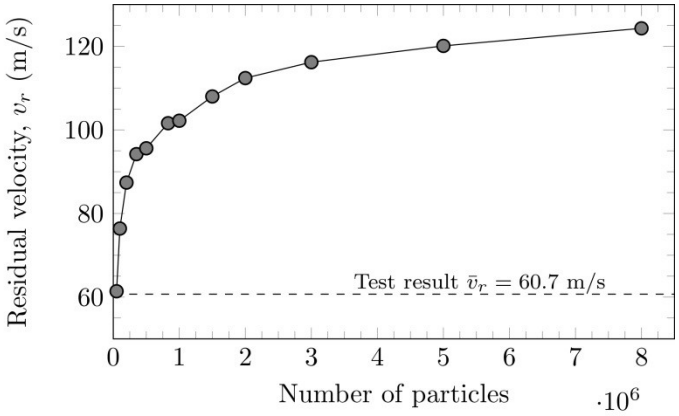

Figure 13: Residual velocity as a function of the number of particles in the calibration model. Note that the x-axis goes from 0 to 8,000,000 particles.

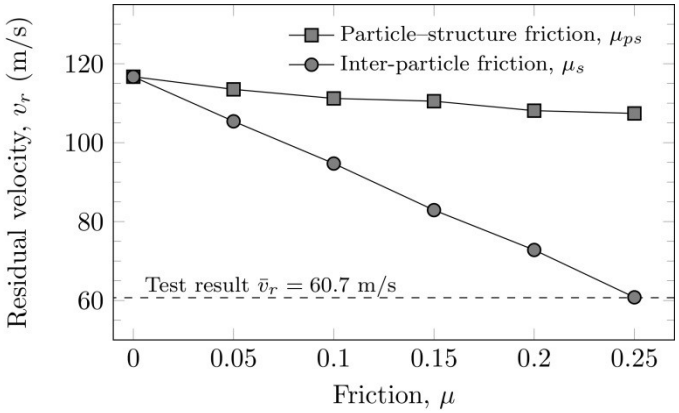

Figure 14: Effects of the inter-particle friction and particle–structure friction in the discrete particle model. The particle diameter is $d = 1.5\,\text{mm}$ (830,000 particles in the calibration model). Note that when μ_{ps} changes μ_p is kept constant, and vice versa.

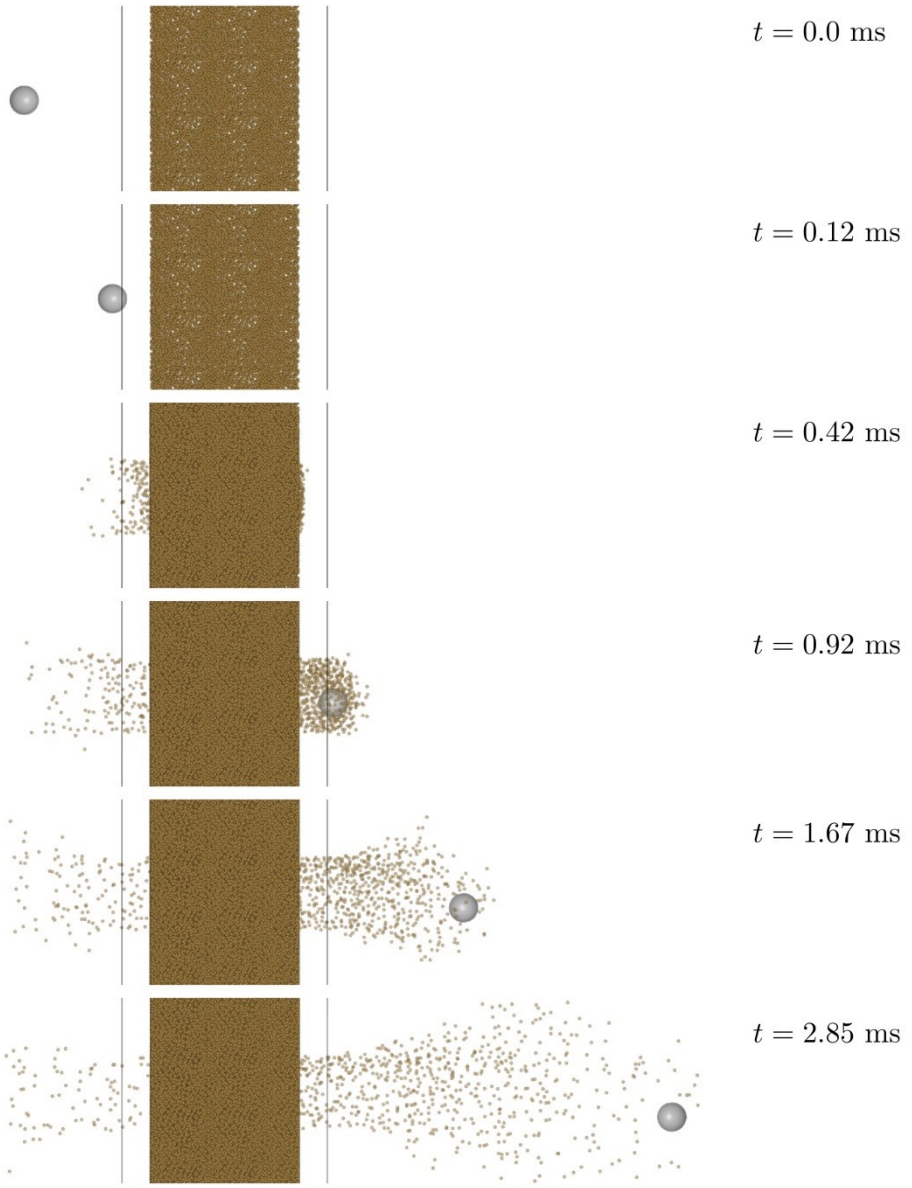

Figure 15: Timelapse from the calibration simulation, $v_i = 279.1\,\text{m/s}$ and $v_r = 62.8\,\text{m/s}$.

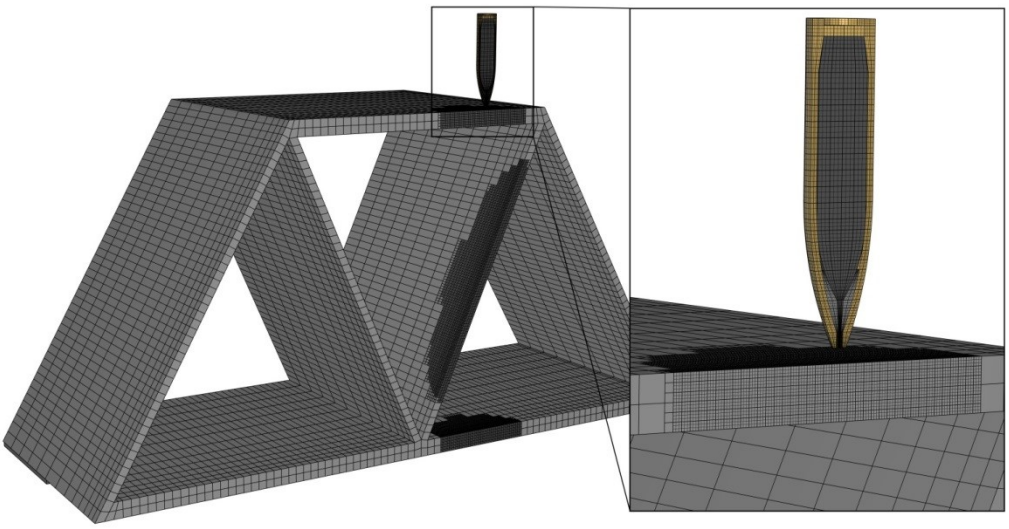

Figure 16: Finite element mesh used for the AA6005-T6 aluminum panels.

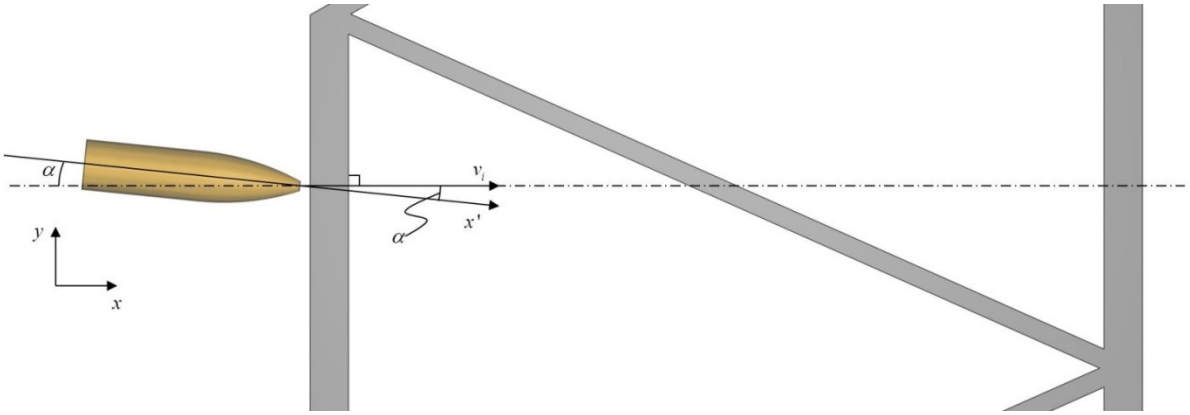

Figure 17: Definition of the positive pitch angle α, where v_i is the initial velocity and x' is in the direction of the centerline of the bullet.

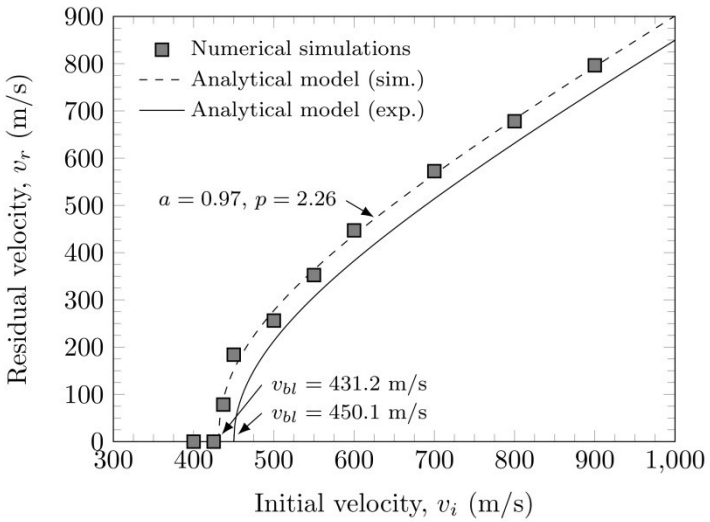

Figure 18: Numerical results from the simulations of the empty aluminum profiles compared to the experimentally fitted analytical model.

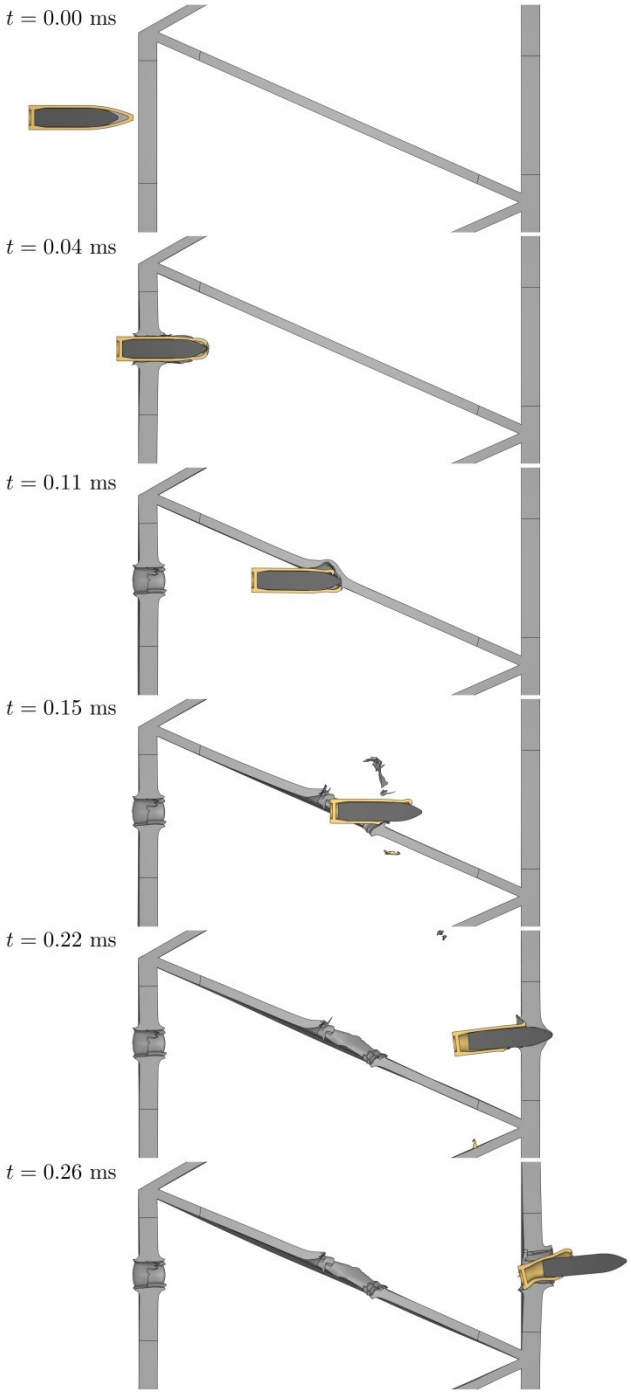

Figure 19: Timelapse of the perforation process of an empty aluminum panel with $v_i = 700\,\mathrm{m/s}$ and $v_r = 572.5\,\mathrm{m/s}$. The panel is cut in half to better illustrate the deformation process.

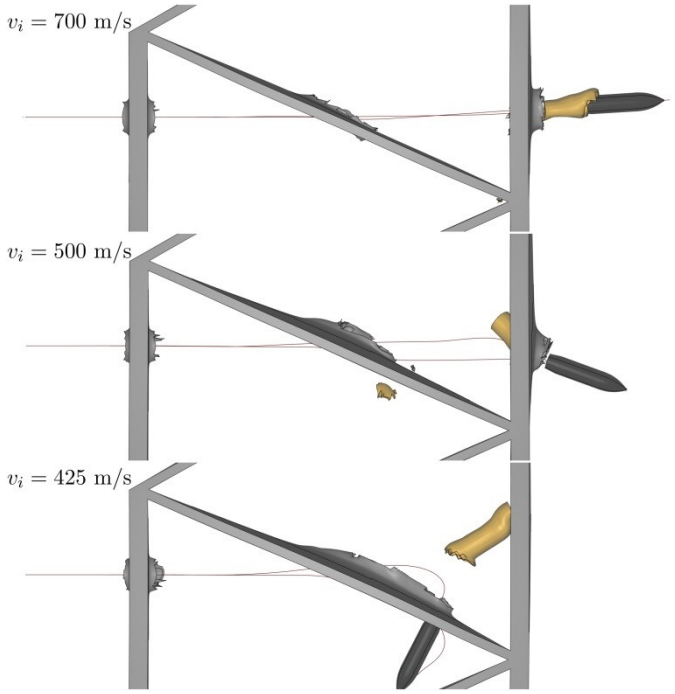

Figure 20: Pictures from the end of a selection of simulations. The lines are the trace of the front-center and rear-center nodes of the rigid core.

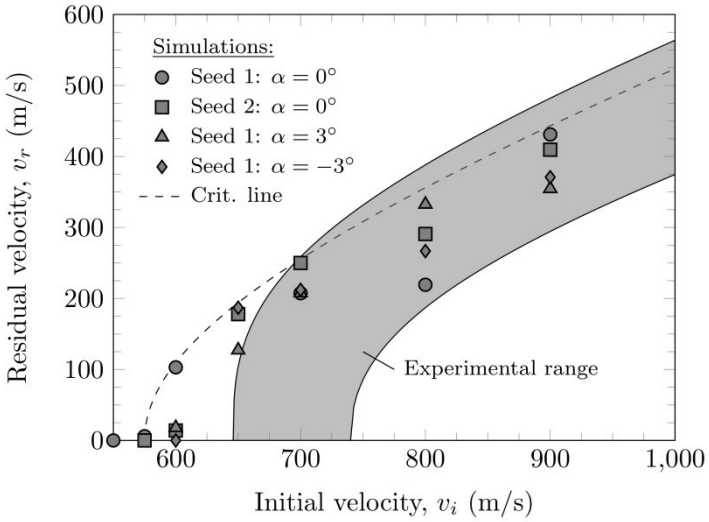

Figure 21: Numerical results from the simulations of the sand-filled aluminum panels.

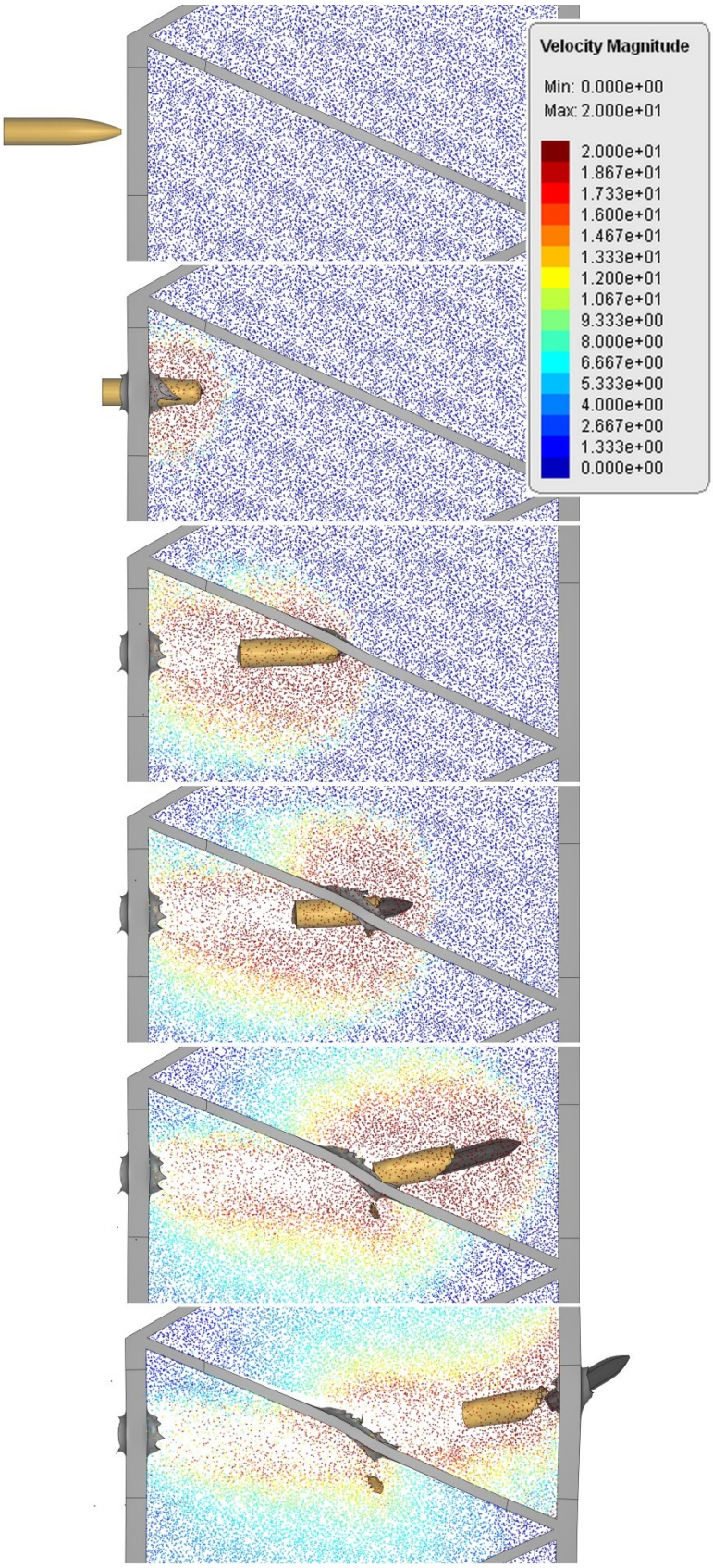

Figure 22: Timelapse of the perforation process and the velocity magnitude of the particles for a sand-filled aluminum panel with $v_i = 700\,\mathrm{m/s}$ and $v_r = 207.4\,\mathrm{m/s}$.

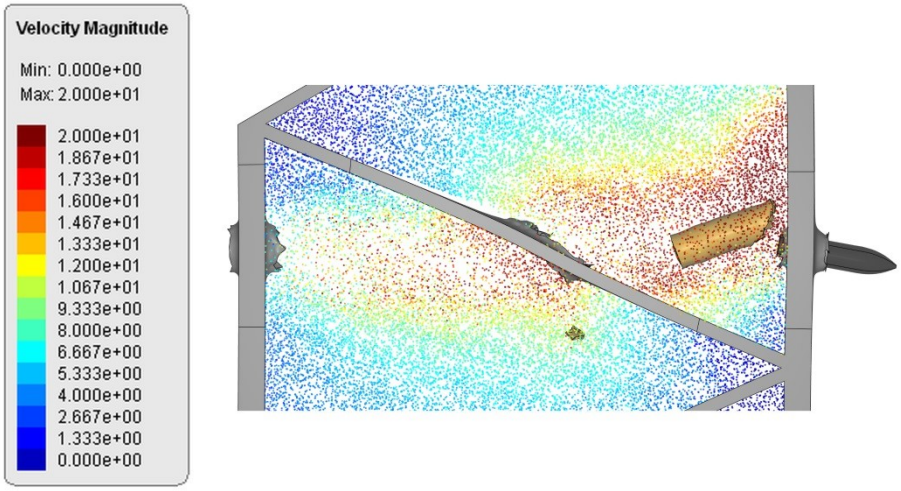

Figure 23: Picture at $t = 0.35$ ms, i.e., the same point in time as the last frame in Figure 22 with the same initial velocity, but different striking point, $v_i = 700$ m/s and $v_r = 250.0$ m/s.

Figure 24: Pictures of an experiment and a simulation of a sand-filled panel to show the qualitative similarities. Left: experiment ($v_i = 910.5$ m/s and $v_r = 485.4$ m/s). Right: simulation ($v_i = 900.0$ m/s and $v_r = 431.0$ m/s).